

# The zonal shift of the Hadley circulation on interannual time scales

Eli Galanti<sup>1</sup>, Dana Raiter<sup>1</sup>, Yohai Kaspi<sup>1</sup>, and Eli Tzipermann<sup>2</sup>

<sup>1</sup>Weizmann Institute of Science

<sup>2</sup>Harvard University

November 22, 2022

## Abstract

Abstract The large scale tropical circulation, commonly named the Hadley circulation, is a key element in the global heat and moisture transport. Traditionally it is defined as the meridional circulation of the zonally averaged flow in the tropics, but in recent years studies have shown the importance of looking at the decomposition of the three-dimensional atmospheric flow into local meridional and zonal circulations. These studies gave useful analysis on the regionality and variability of the meridional circulation in different time scales, but were mostly limited to examining the regional strengthening/weakening of the circulation. Here we study the interannual variability of the longitudinally-dependent meridional circulation (LMC), with a focus on its zonal shift. We use hierarchical clustering to objectively determine the 5 main modes of the LMC interannual variability, and apply a Lagrangian air parcel tracking method to reveal the detailed patterns of the circulation. We find that the most prominent interannual variability of the LMC is an east-west shift, which plays a dominant role in the overall interannual variability of the tropical circulation. In addition, the LMC variability is found to be strongly related to other atmospheric variables such as the sea surface temperature, precipitation and air temperature. Using multiple linear regression we analyze these dependencies and discuss their implications for the tropical climate system. We also relate the LMC interannual variability to the Madden-Julian Oscillation (MJO) and find that the 2 La-Nina related modes are significantly correlated with 2 different MJO phases.

# The zonal shift of the Hadley circulation on interannual time scales

Eli Galanti<sup>1</sup>, Dana Raiter<sup>1</sup>, Yohai Kaspi<sup>1</sup>, and Eli Tziperman<sup>2</sup>  
(Submitted to JGR-Atmosphere)

March 13, 2021

<sup>1</sup>*Department of Earth and Planetary Sciences, Weizmann Institute of Science, Rehovot, Israel.*

<sup>2</sup>*Department of Earth and Planetary Sciences, Harvard University, Cambridge, MA, USA*

## Abstract

The large-scale tropical circulation, commonly named the Hadley circulation, is a key element in the global heat and moisture transport. Traditionally it is defined as the meridional circulation of the zonally averaged flow in the tropics, but in recent years studies have shown the importance of looking at the decomposition of the three-dimensional atmospheric flow into local meridional and zonal circulations. These studies gave useful analysis on the regionality and variability of the meridional circulation in different time scales, but were mostly limited to examining the regional strengthening/weakening of the circulation. Here we study the interannual variability of the longitudinally-dependent meridional circulation (LMC), with a focus on its zonal shift. We use hierarchical clustering to objectively determine the 5 main modes of the LMC interannual variability, and apply a Lagrangian air parcel tracking method to reveal the detailed patterns of the circulation. We find that the most prominent interannual variability of the LMC is an east-west shift, which plays a dominant role in the overall interannual variability of the tropical circulation. In addition, the LMC variability is found to be strongly related to other atmospheric variables such as the sea surface temperature, precipitation and air temperature. Using multiple linear regression we analyze these dependencies and discuss their implications for the tropical climate system. We also relate the LMC interannual variability to the Madden-Julian Oscillation (MJO) and find that the 2 La-Niña related modes are significantly correlated with 2 different MJO phases.

## 1 Introduction

The Hadley circulation is a key element of the climate system [Hartmann, 1994], responsible for the energy and moisture transport from the equatorial region to the subtropics [e.g., Trenberth and Stepaniak, 2003]. The circulation is commonly defined as the zonally-averaged meridional circulation in the tropical region [Hartmann, 2016], and is usually calculated as an annual mean or as an average over specific months or seasons.

The large longitudinal variations in the different elements involved in the Hadley circulation, such as the strength of the Inter Tropical Convergence Zone (ITCZ) and the location of the subtropical jets that mark the edge of the Hadley circulation, led to the need to calculate the contributions to the Hadley circulation at different longitudes. A method for calculating localized 2D circulations from the 3D wind field was first introduced by Keyser *et al.* [1989]. Decomposing the wind field into a rotational and divergent components (Helmholtz decomposition), the longitudinally-dependent circulation can be derived from the divergent part of the flow. This method was implemented in several studies for the analysis of the the Hadley and Walker circulations in specific longitudinal sectors. It was first used to define the horizontal velocity potential and divergent wind in the upper troposphere, in which both the meridional circulation (Hadley) and the zonal circulation (Walker) are manifested. This definition enabled the investigation of the global monsoon system and its relation to the Hadley and Walker circulations on seasonal to decadal time scales [Trenberth *et al.*, 2000; Tanaka *et al.*, 2004].

Decomposing the flow field into a local meridional and zonal circulations was used to calculate the relative contributions of the vertical mass fluxes in the middle-troposphere to the Hadley and Walker circulations [Schwendike *et al.*, 2014]. The spatial distribution of vertical and meridional velocities were used also to calculate trajectories of climatological flow emphasizing the regional aspects of the Hadley circulation [Karnauskas and Ummenhofer, 2014]. Examining the interannual variability of the different circulations, Schwendike *et al.* [2014] found that ENSO has a much larger effect on the local Hadley circulation than on the local Walker circulation. This study was performed

44 over specific longitudinal and latitudinal sectors, focusing on the Maritime continent. The same methodology was  
 45 later used to study the inter-decadal trend of both the Hadley and Walker circulations [Schwendike et al., 2015],  
 46 where it was shown that in order to understand the effect of climate variability on the tropical circulation patterns  
 47 the analysis should be regional. The longitudinally-dependent Hadley and Walker circulations were also found to  
 48 have correlation with different phases of the Madden-Julian Oscillation [Schwendike et al., 2021]. The same method  
 49 was also used to study specific regions of interest, such as the Atlantic sector of the Hadley circulation during  
 50 the Boreal summer and its connection to the Atlantic tropical cyclone activity [Zhang and Wang, 2013], and the  
 51 variability of the Hadley circulation in the Southern Hemisphere in different sectors of the world [Nguyen et al.,  
 52 2018]. The method was also compared to a more general 3D decomposition of global atmospheric circulation [Hu  
 53 et al., 2017]. More recently, Raiter et al. [2020] used the same method, combined with a Lagrangian tracking of air  
 54 parcels, to examine in detail the mean tropical circulation, showing how the longitudinally-dependent meridional  
 55 circulation is acting together with the subtropical jets to produce a tropical atmospheric conveyer belt.

56 In all these studies, two main perspectives were used to examine the local meridional circulation. Some studies  
 57 analyzed latitude-longitude maps of the vertical mass flux in the middle-troposphere or the divergent flow at the  
 58 upper troposphere. Other studies analyzed latitude-pressure maps of the meridional circulation itself hence it was  
 59 necessary to average the circulation over a longitudinal sector, making a full 3D global view impossible. Another  
 60 limitation of past studies was the methodology used for investigating the interannual variability, which was defined  
 61 based on other modes of variability in the tropical region, for example a state of El-Niño or a state of La-Niña . This  
 62 makes the variability of the Hadley circulation a mere reflection of the other modes of variability. Therefore, there  
 63 is a need to define the modes of interannual variability of the Hadley circulation with a more objective method.

64 Here we study the interannual variability of the longitudinally-dependent meridional circulation (LMC) with  
 65 a focus on the zonal shift it exhibits on interannual time scales. We perform the study using clustering analysis,  
 66 allowing an objective determination of the most important modes of variability without restricting the analysis to  
 67 ENSO-related modes. In addition, we use a Lagrangian perspective to tie these modes to the actual 3D changes in  
 68 the air flow. Finally, we investigate the connection between the LMC and other variables of the tropical climate  
 69 system, such as the sea surface temperature, precipitation, air temperature, and the Madden-Julian Oscillation.

70 The manuscript is organized as follows: in section 2 we present the method by which the local meridional  
 71 circulation is calculated and the method for clustering its interannual variability. The results are shown in section 3,  
 72 with the zonal shift discussed in section 3.1, and the relation to other climatic variables discussed in section 3.2.  
 73 We conclude in section 4.

## 74 2 Data and methods

### 75 2.1 The longitudinally-dependent meridional circulation

76 We use two data sets to ensure robustness of our analysis: the European Center for Medium range Weather Forecasts  
 77 ERA-Interim reanalysis [Dee et al., 2013], and the National Centers for Environmental Prediction (NCEP) reanalysis  
 78 II [Kanamitsu et al., 2002], both provide 6-hourly data, covering the years 1979-2018. In this section we show the  
 79 analysis of the first data set, and the interannual variability analysis we use both. The mass-weighted global  
 80 meridional circulation [Hartmann, 2016] is represented by a stream function calculated using the zonally-averaged  
 81 meridional velocity  $\bar{v}$

$$\psi(\theta, p, t) = \frac{2\pi a \cos \theta}{g} \int_0^p \bar{v}(\theta, p', t) dp', \quad (1)$$

82 where  $a$  is Earth's radius,  $g$  is the gravitational acceleration,  $\theta$  is latitude, and  $p$  is pressure. The time average of  
 83 this circulation is shown in Fig. 1a. The two classical Hadley cells can be seen between the equator and latitudes  
 84  $\pm 30^\circ$ . Taking the average of the stream function between 400 – 600 hPa, where the stream function reaches its  
 85 maximum [Nguyen et al., 2013], the time dependency is revealed (Fig. 1b), with the Hadley circulation alternating  
 86 seasonally between the hemispheres. However, the circulation, as defined by Eq. 1, cannot account for any zonal  
 87 asymmetry in the meridional circulation. The longitudinally-dependent meridional circulation can be calculated  
 88 via the separation of the 3D wind velocity field into a meridional component and a zonal one. Here we follow the  
 89 notation of Hu et al. [2017]. First, the divergence of the wind is calculated

$$D = \nabla \cdot \vec{V}, \quad (2)$$

90 where  $\vec{V} = (u, v)$  is the full horizontal wind vector. Then, the velocity potential  $\chi$  is calculated via

$$\nabla^2 \chi = D. \quad (3)$$

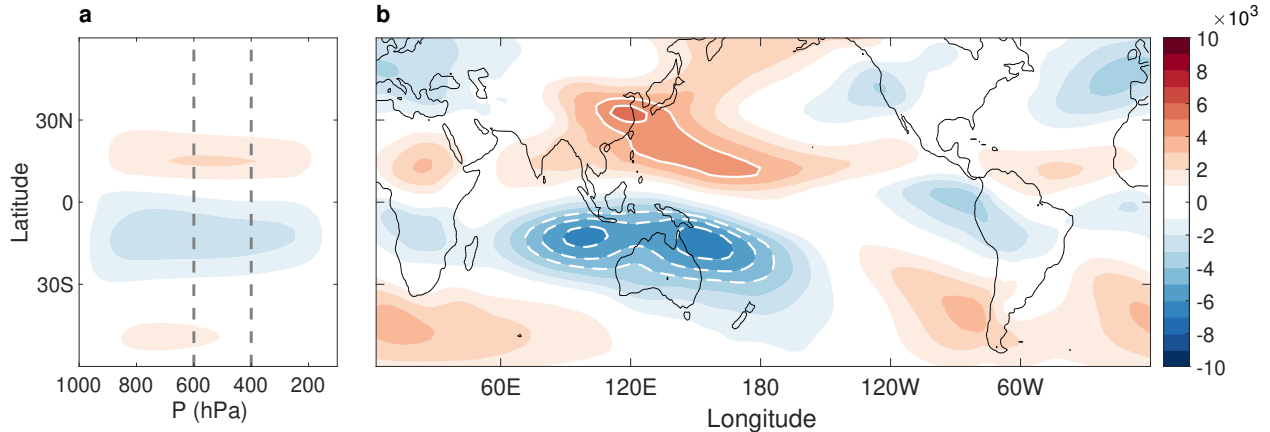


Figure 1: The climatological meridional circulation. (a) The zonally averaged circulation as function of latitude and pressure with the dashed lines denoting the 400 and 600 hPa. (b) The annual average of the meridional longitudinally-dependent circulation, averaged between 400 and 600 hPa, as function of longitude and latitude. Contour interval is  $1 \times 10^3 \text{ kg s}^{-1} \text{ m}^{-1}$ . White solid and dashed lines indicate absolute values larger than  $4 \times 10^3 \text{ kg s}^{-1} \text{ m}^{-1}$ .

91 This equation can be solved either via decomposition into spherical harmonics, or by formulating the problem as a  
 92 set of finite difference linear equations and inverting the Laplacian. The methods are equivalent and in this study  
 93 the latter is used. The potential function is then used to calculate the divergent wind

$$\nabla\chi = \vec{V}_{\text{div}}, \quad (4)$$

94 where  $\vec{V}_{\text{div}} = (u_{\text{div}}, v_{\text{div}})$ . The zonal (meridional) component of the divergent wind is associated with east-west  
 95 (north-south) closed oriented circulations, such as the Walker (Hadley) cell. Therefore, the divergent wind can be  
 96 used, similar to Eq. 1, to calculate the longitudinally-dependent meridional circulation

$$\psi(\phi, \theta, p, t) = \frac{1}{g} \int_0^p v_{\text{div}}(\phi, \theta, p', t) dp'. \quad (5)$$

97 Note that the integral of Eq. 5 over longitude gives the classical zonally averaged meridional circulation (Eq. 1). A  
 98 simplified representation of the meridional circulation can be defined by averaging  $\psi$  between 600 – 400 hPa

$$\tilde{\psi}(\phi, \theta, t) = \frac{1}{\Delta p} \int_{p_1}^{p_2} \psi(\phi, \theta, p', t) dp', \quad (6)$$

99 where  $p_1 = 400 \text{ hPa}$ ,  $p_2 = 600 \text{ hPa}$ , and  $\Delta p = p_2 - p_1$ . As discussed above this is the region where the meridional  
 100 circulation reaches its maximum. We will use this simplified definition of the local meridional circulation (denoted  
 101 hereafter as LMC) throughout this study. The time averaged LMC is shown in Fig. 1b. It has a very strong zonal  
 102 dependence - it is most pronounced in the Indo-Pacific region, between  $70^\circ - 180^\circ\text{E}$ , and is much stronger in the  
 103 Southern hemisphere.

## 104 2.2 Interannual variability analysis using hierarchical clustering

105 The temporal variability of the LMC can be explored using cluster analysis, in which spatial patterns that are  
 106 prone to repeat in time are identified. Unlike methods based on principle components requiring that the different  
 107 patterns are orthogonal to each other, clustering allows the identification of commonly occurring patterns that may  
 108 not be orthogonal. There are several methods to perform cluster analysis, we use hierarchical clustering that was  
 109 successfully applied to the studies of atmospheric dynamics [e.g., *Cheng and Wallace*, 1993; *Totz et al.*, 2017; *Horton*  
 110 *et al.*, 2015]. Other variants of the clustering method such as the *k-means* [e.g., *Madonna et al.*, 2017] and self  
 111 organizing maps [e.g., *Feldstein and Lee*, 2014] were used in climate studies. The data use here - the monthly-mean  
 112 longitudinally-dependent meridional circulation at each time step averaged over 400 – 600 hPa, is treated as an  $N$

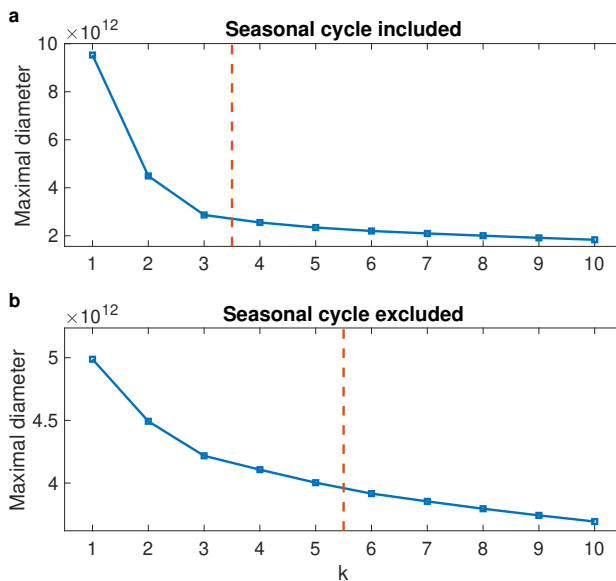


Figure 2: Maximal cluster diameter as function of the number of clusters used in the analysis. (a) for the full LMC, and (b) for the LMC after removal of the seasonal cycle. Dashed red lines denote the cutoff used in each case: 3 clusters for the seasonal cycle and 5 for the interannual variability.

113 dimensional vector where  $N$  is the number of grid points. Since we are using two data sets, the number of samples  
 114 is twice the time span. The method allows to find how the 960 vectors are clustered in the  $N$ -dimensional space.  
 115 Starting with the assumption that each point of the entire data set is a single cluster, the method then performs a  
 116 hierarchical separation of the data to a decreasing number of clusters, combining previously identified clusters into  
 117 new clusters using the Ward method [Wilks, 2011]. One then needs to decide what the optimal number of clusters  
 118 is.

119 Plotting the maximal cluster diameter (the largest Euclidean distance between the vectors within a given cluster)  
 120 as function of the number of clusters, the optimal number of clusters can be identified. Fig. 2a shows the maximal  
 121 diameter as function of number of clusters used in the analysis. The smaller this maximum diameter is, the more  
 122 similar members of each cluster are to each other. By definition, increasing the number of clusters results in a  
 123 smaller maximal diameter (vectors are better clumped together). However, it is evident that the maximum cluster  
 124 diameter decreases substantially in the range up to 3 clusters, while further increasing the number of clusters does  
 125 not result in a significant reduction. As expected, 3 clusters are sufficient to describe the first order time variability  
 126 of the LMC, composing the seasonal cycle of the circulation (winter, summer, and autumn/spring).

127 Removing the seasonal cycle from the data (via the subtraction of the twelve monthly averages from the corre-  
 128 sponding points of the monthly data), the number of leading clusters associated with the interannual variability of  
 129 the circulation can be identified (Fig. 2b). Here, there is no clear jump in the maximal diameter, and it was found  
 130 out that an analysis with 5 clusters gives the most efficient, yet comprehensive, of the LMC interannual variability.  
 131 Finally, given the assignments of the monthly data to the different clusters a composite field can be calculated for  
 132 each of these clusters. Note that even though the different clusters might be assigned to different months in the two  
 133 data sets (ERA-Interim and NCEP), in practice each of the 5 clusters are found to be assigned to exactly the same  
 134 months in the two data sets. Moreover, all the results discussed in this study are evident in both data sets, i.e., the  
 135 composites calculated for each cluster are very similar, ensuring the robustness of the results. For convenience we  
 136 show the analysis of the ERA-Interim data.

### 137 3 Results

138 We start by examining the temporal variability of the different clusters identified. by Fig. 3a shows the occurrence of  
 139 the 5 clusters  $C_1, \dots, C_5$  in different colors, on top of the Oceanic Niño Index (ONI, a 3 month running mean of SST  
 140 anomalies in the Niño 3.4 region of  $5^\circ\text{N}$ - $5^\circ\text{S}$ ,  $120^\circ$ - $170^\circ\text{W}$ ). The ONI represents the El-Niño Southern Oscillation  
 141 (ENSO) phenomenon that is the prime interannual variability in the tropical region. The first cluster appear mostly  
 142 during a time with neutral or weak ENSO conditions, with an occurrence of 37%. The second cluster appear mostly

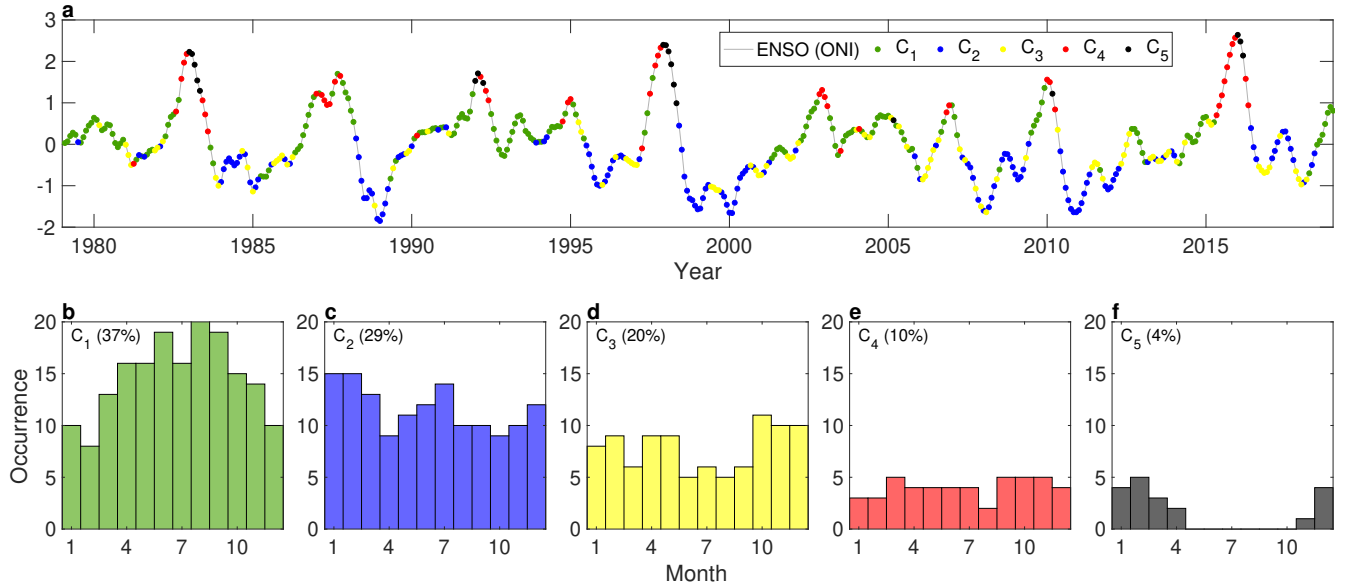


Figure 3: The time occurrence of the LMC interannual variability clusters. (a) the occurrence of each cluster plotted as colored dots on top of the ENSO ONI index. (b-f) the occurrence of each cluster as function of the month of the year. Also shown is the total occurrence percentage of each cluster.

143 during strong La-Niña conditions with occurrence of 29%, and the third cluster appear mostly during weak La-Niña  
 144 conditions with occurrence of 20%. The fourth and fifth clusters can be related to El-Niño conditions, with the latter  
 145 capturing the more extreme El-Niño conditions. The overall occurrence of the El-Niño related clusters is 14% .  
 146 Also interesting is the occurrence of the clusters as function of the month of the year (Fig. 3b-f). The occurrence  
 147 of clusters  $C_1$  is more frequent during the northern hemisphere summer while  $C_5$  appears only during the northern  
 148 hemisphere winter (peak of strong El-Niño events). On the other hand, the occurrence of clusters  $C_2$ ,  $C_3$ , and  $C_4$   
 149 has only a weak dependence on the month of the year. Therefore it seems that the seasonality preference of the  
 150 strong El-Niño events (cluster  $C_5$ ) is compensated by the neutral/weak conditions of cluster  $C_1$ .

### 151 3.1 The zonal shift in the meridional circulation

152 Based on the classification of each of the 480 months, a composite of the LMC is calculated for each cluster from the  
 153 IRA-Interim data set (Fig. 4a-e). Composites based on the NCEP Reanalysis gives very similar spatial patterns.  
 154 For each composite we calculate the 95% confidence level using a non-parametric two-sided statistical test where  
 155 the absolute value of the cluster at each grid point is checked to be larger than the one calculated with a random  
 156 selection of months, 95% of the times. Marking the regions where the results are not statistically significant with  
 157 gray dots, it is clear that the cluster structure is significant in all regions where the clusters have large values.

158 The clusters all have a strong north-south asymmetry around the equator, an indication of a change in the  
 159 strength in both the northern and southern hemisphere LMC, but also an east-west asymmetry, peaking around a  
 160 longitude range between 90°E and 150°W . This pattern of two maxima and two minima indicates a shift of the  
 161 LMC either eastward ( $C_1$ ,  $C_4$  and  $C_5$ ) or westward ( $C_2$  and  $C_3$ ) relative to climatology. This zonal movement of  
 162 the Hadley circulation was not observed previously and its identification is made possible due to the definition of  
 163 the LMC made in this study.

164 As the LMC captures only the meridional component of the tropical large-scale circulation, a better under-  
 165 standing of the changes on interannual time scales in the actual 3D circulation can be achieved with a Lagrangian  
 166 perspective, in which air parcels trajectories are followed given an initial position [Raiter et al., 2020]. Based on  
 167 the cluster analysis (Fig. 4a-e), we set two regions of initial positions around the equator, one between 90°E and  
 168 150°E, and another between 150°E and 150°W (Fig. 5, black dots). These regions cover the main dipole signal  
 169 in the 5 clusters. For simplicity, we examine the circulation in a climatological state (upper panels), an El-Niño  
 170 related state composed from clusters  $C_4$  and  $C_5$  months (middle panels), and a La-Niña related state composed from  
 171 cluster  $C_2$  months (lower panels). Since the tropical circulation has a significant seasonal cycle, we define the states  
 172 using only the DJF months, but a similar behavior (in the opposite hemisphere) is apparent when looking at the  
 173 JJA months. The air parcels initial positions are set at a height of 500 hPa, and are followed for 20 days forward

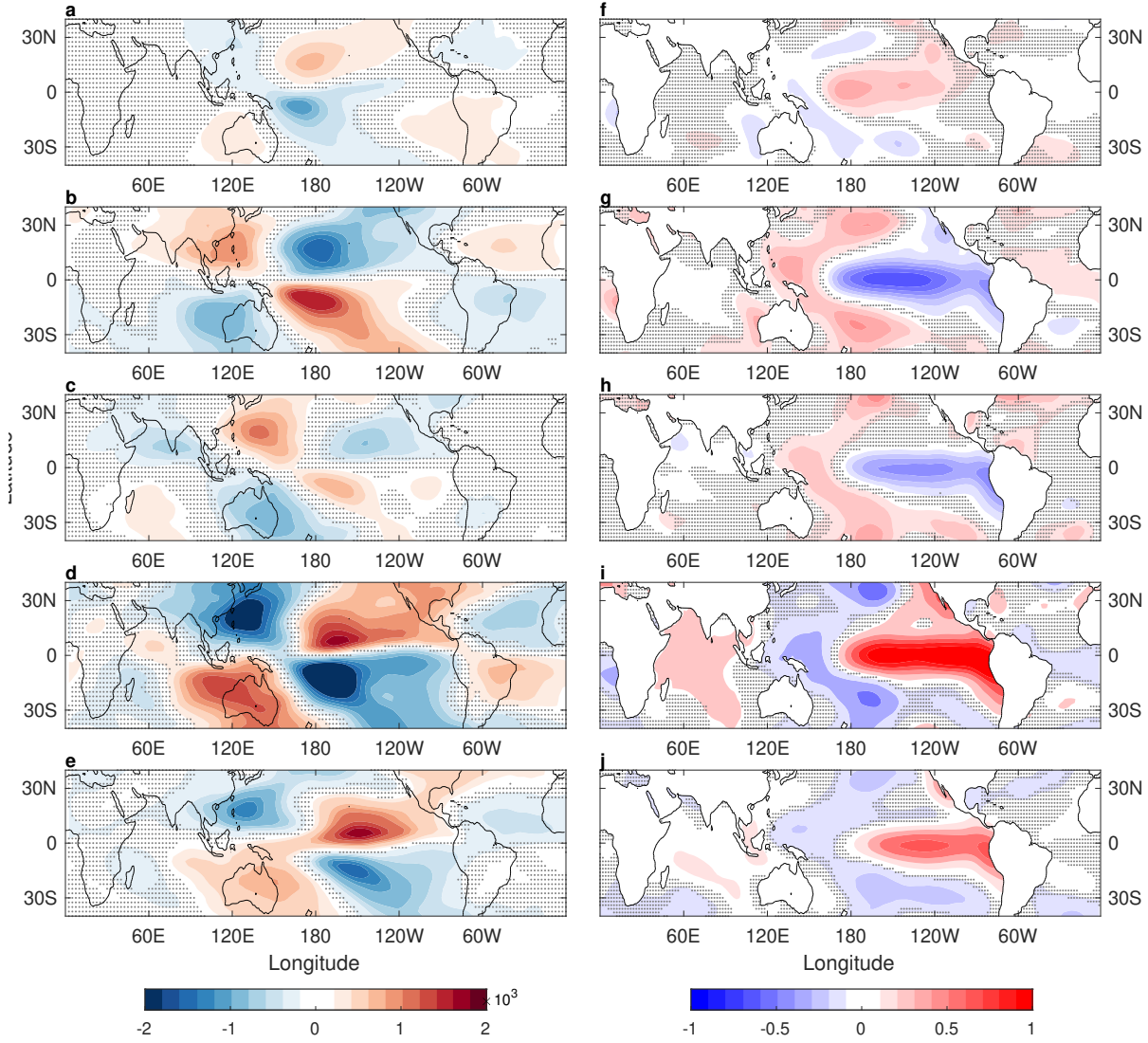


Figure 4: (a-e) Composites of the anomalous LMC for each of the 5 clusters (in  $\text{kg s}^{-1} \text{m}^{-1}$ ). (f-j) Composites of SST anomalies for each of the clusters (in  $^{\circ}\text{C}$ ). Dotted areas indicate regions where the cluster is not statistically significant. Note that the values in (e) and (j) are reduced by factor of 3 to match the scale of the other clusters.

174 and 20 days backward in time. This allows a sufficient coverage of the full tropical circulation (see *Raiter et al.*  
 175 2020 for a detailed discussion of the methodology).

176 Stating from the DJF climatological state (Fig. 5, upper panels), the northern hemisphere longitudinally-  
 177 dependent Hadley circulation is apparent. The air, raising in the maritime continent, moves northward with  
 178 the meridional circulation, and then enters the jet streams moving eastward. Part of the circulation descends in the  
 179 mid-Pacific and part descends over the Americas. The backward trajectories show how the air is converging to the  
 180 equatorial region from the lower altitude central and eastern Pacific. The interannual variability is clearly seen in  
 181 the ENSO related states. During El-Niño related months (middle panels), the western region (left panels) exhibits  
 182 weaker and more confined circulation, while the eastern region (right panels) exhibits a much more pronounced  
 183 meridional circulation. In fact, while in the climatological state the air parcels either move to the west Pacific before  
 184 going north or stay close to their initial position, during the El-Niño conditions the air parcels move directly up and  
 185 north. Conversely, during La-Niña conditions (lower panels) the air parcels originating in the western region exhibit  
 186 much stronger circulation that extends over a larger region than in the climatological conditions. The circulation  
 187 of the air parcels originating from the eastern region is again very different from the climatological circulation,  
 188 with the air parcels moving to the west before rising and moving north. The east-west shift is also apparent in the back  
 189 trajectories of the La-Niña conditions, where very weak convergence is seen in the eastern region. Therefore, we  
 190 find that the full tropical circulation shifts in the east-west direction on interannual time scales, and is dominated

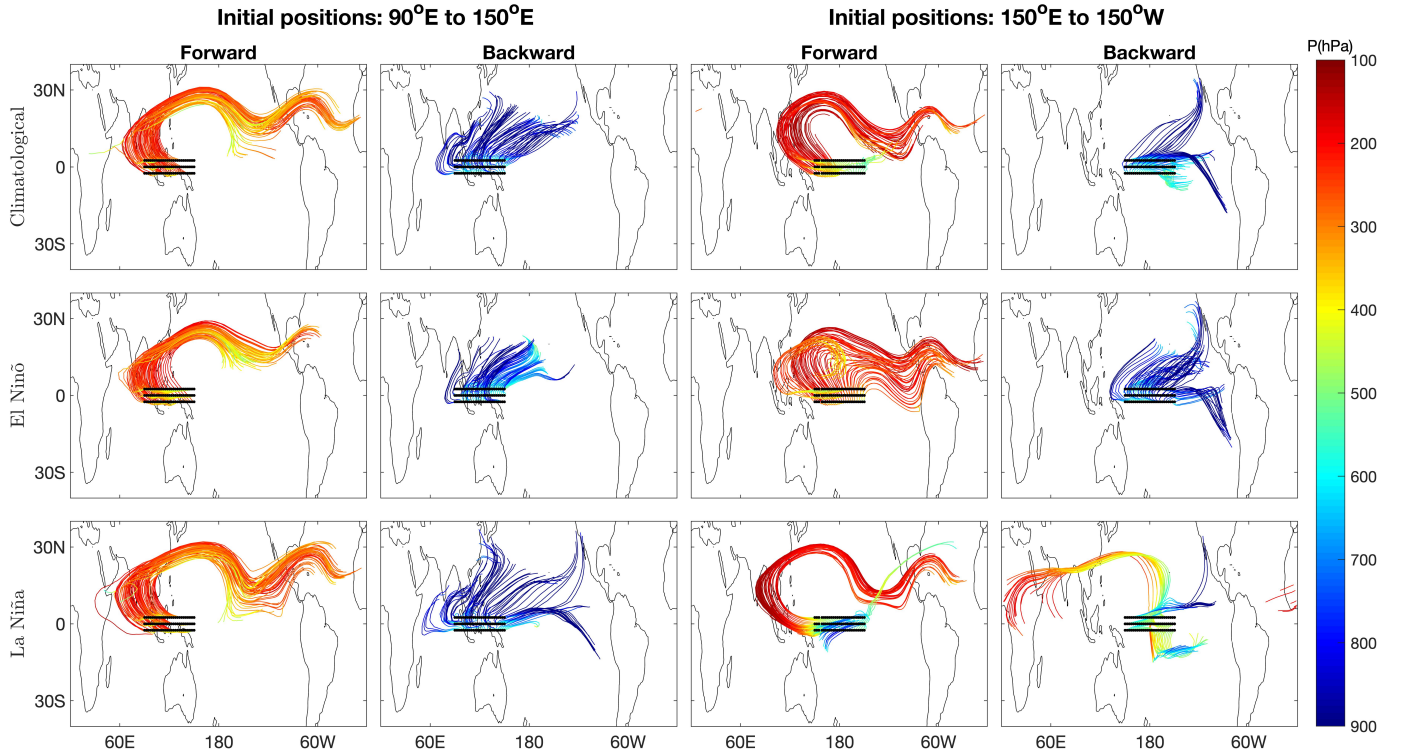


Figure 5: Trajectories of air parcels during DJF climatological conditions (upper panels), El-Niño conditions (middle panels), and La-Niña conditions (lower panels). Initial positions are set around the equator in two main regions: 90°E to 150°E, and 150°E to 150°W. The air parcels are initiated from a height of 500 hPa and followed for 20 days forward, and 20 days backward. The color indicate the height (hPa) of the parcel during it trajectory.

191 by the east-west shift in the LMC.

### 192 3.2 Connection to other atmospheric variables

193 The classification of the temporal variations of the LMC into the 5 clusters can be used to search for accompanying  
 194 variability in other atmospheric variables. Given that ENSO is the dominant interannual variability in the tropical  
 195 region and was already identified as correlated with the LMC (Fig. 3a), we calculate the composites for the SST  
 196 anomalies (seasonal cycle removed similarly to the LMC) for each of the clusters (Fig. 4f-j). The ENSO signal is  
 197 clearly identified in the strong SST anomalies at the central to east equatorial Pacific, with  $C_2$  and  $C_3$  associated  
 198 with a La-Niña phases and  $C_4$  and  $C_5$  with an El-Niño phases. Note that  $C_3$  ( $C_2$ ) relates to a more western (central)  
 199 Pacific phase of La-Niña, and  $C_4$  ( $C_5$ ) relates to a more central (eastern) Pacific phase of El-Niño . Finally, the  
 200 cluster  $C_1$  only has a weak signal in the SST anomalies that is more western than the other El-Niño related clusters.

201 Cluster  $C_5$  is unique as it represents only the months where strong El-Niño events reach their peak, which  
 202 appears only during the months November-April and occurs only 4% of the time (Fig. 3f). As a result, the composite  
 203 amplitudes of both the LMC and the SST anomalies are much larger than for the other clusters, therefore in Fig. 4e  
 204 and Fig. 4j the values were scaled down by a factor of 3 to allow them to be shown on the same scale as the other  
 205 clusters. To summarize, a strong connection to ENSO is found, with 2 clusters associated with two different El-Niño  
 206 phases, 2 clusters with two different La-Niña phases, and one cluster that seems to be weakly related to positive  
 207 SST.

208 Next, we examine whether we can relate the variability in the LMC to variability in the climate system, repre-  
 209 sented by the air temperature at 2 meters and the total precipitation. The composites for the two fields is shown  
 210 in Fig. 6. The composites in both fields are statistically significant where the amplitude is substantial, indicating  
 211 that the interannual variability of both air temperature and precipitation is strongly correlated with the LMC  
 212 variability. However, there are major differences between the fields, while the precipitation variability (Fig. 6f-j)  
 213 is mostly confined to the equatorial region and to a zonal region that is similar to the spatial structures involved in  
 214 the LMC variability (Fig. 4a-e), the variability in the air temperature (Fig. 6a-e) is much broader, reaching higher

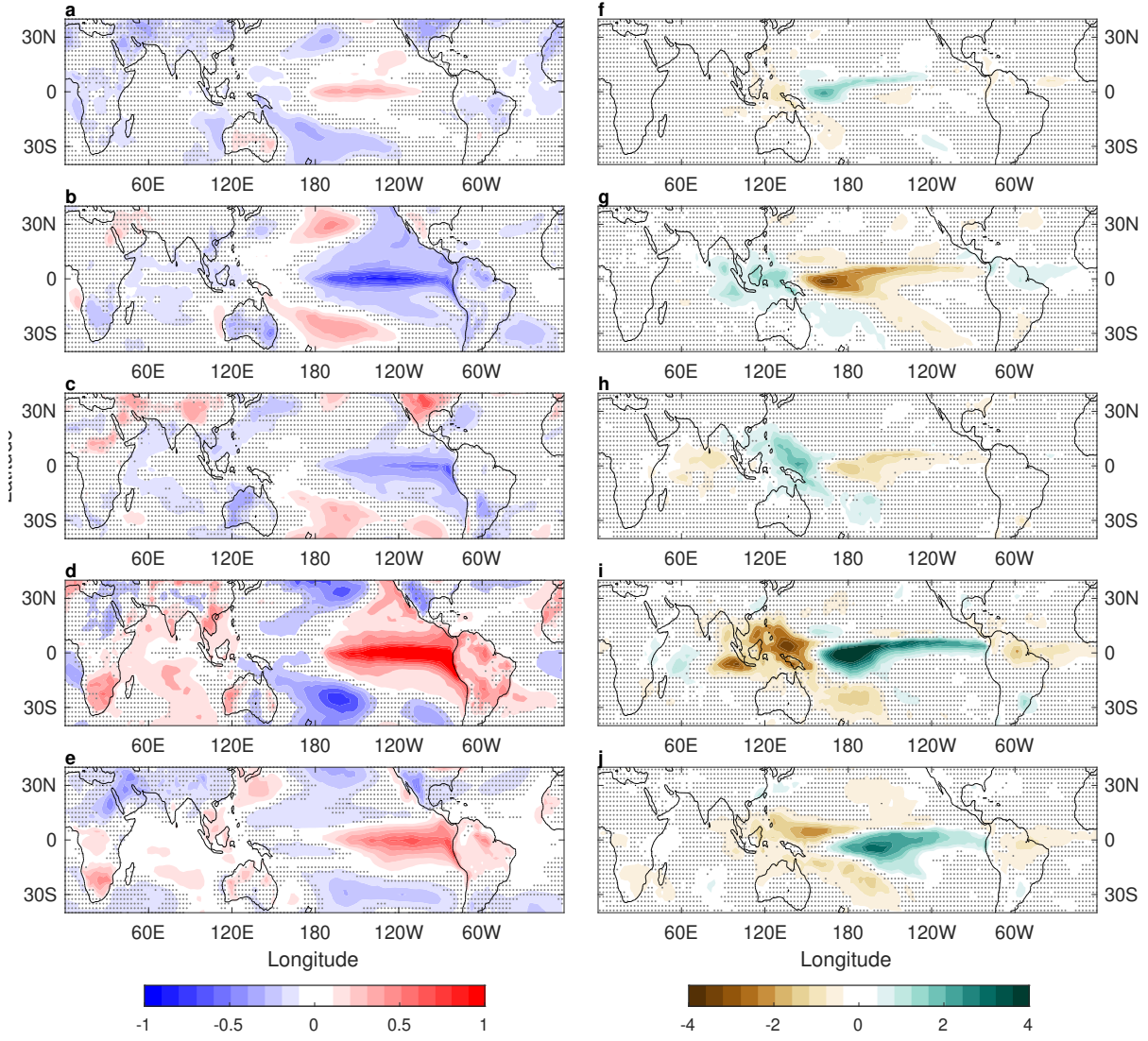


Figure 6: Same as in Fig. 4 but (a-e) for the 2 meter air temperature (in  $^{\circ}\text{C}$ ), and (f-j) for the total precipitation (in  $\text{mm day}^{-1}$ ). Note that the values in (e) and (j) are reduced by a factor of 3 to match the scale of the other clusters.

latitudes as well.

The large-scale variability of the LMC is indeed expected to be strongly correlated with the SST variability due to the robust ocean-atmosphere interaction in the tropics. However, it is not clear whether the statistically significant composites of the air temperature and precipitation are a result of the variability in the LMC or a direct response to the SST. We examine this via the connection between time series representing the variability in all four fields. For this purpose, the LMC is projected on each of its composites,

$$\tilde{\psi}_i(t) = \frac{1}{2\pi\Delta\theta} \int_{\theta=-\frac{\pi}{3}}^{\frac{\pi}{3}} \int_{\phi=0}^{2\pi} \tilde{\psi}(\phi, \theta, t) C_i(\phi, \theta) \cos\theta d\phi d\theta, \quad (7)$$

and the resulting time series are then normalized by their standard deviation. Similarly, all other fields are projected onto their respective composites and normalized. A section of the resulting time series of the air temperature, precipitation, LMC and SST are shown in Fig. 7. While the overall behavior in time of all fields is similar, there are small time scale differences that may be a result of stronger dependencies between some of them. For each cluster, we calculate the multiple linear regression between the temperature or precipitation and the LMC and SST,

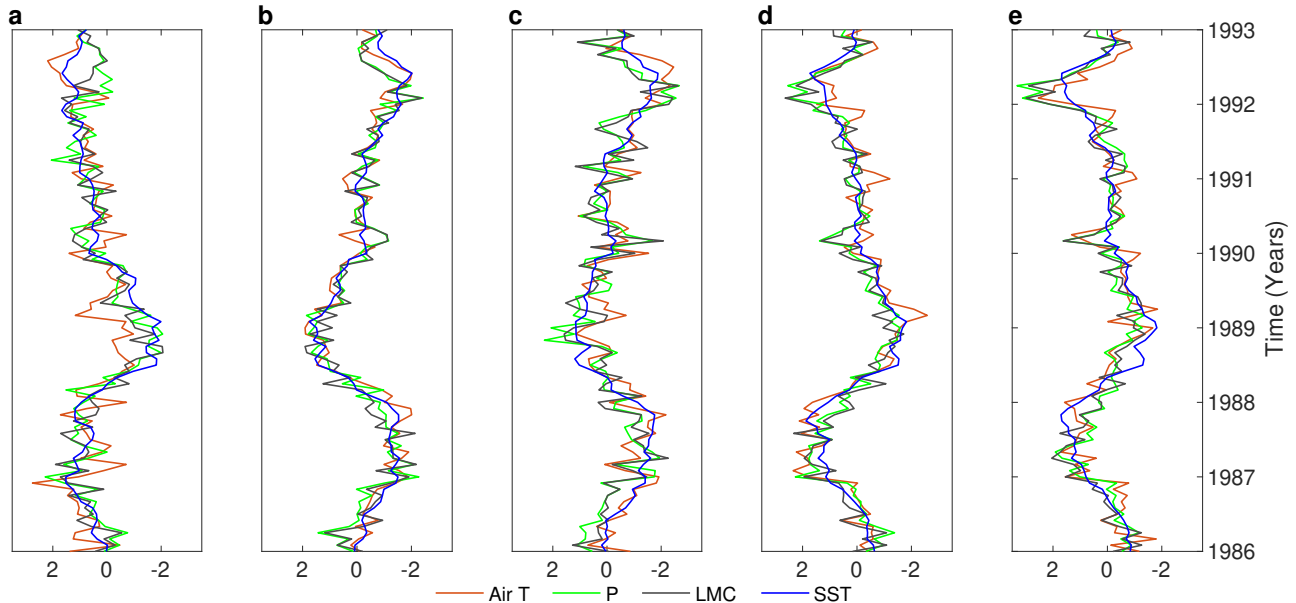


Figure 7: The projection of the 2 meter air temperature (red), total precipitation (green), LMC (red) and SST (blue) onto their 5 respective composites (a-e). For a better view of the temporal behavior we show a subsection of the data covering 1986-1993.

226 to give a dependency of the form

$$AirT(t) = \alpha_T + \beta_T LMC(t) + \gamma_T SST(t) \quad (8)$$

227 and

$$P(t) = \alpha_P + \beta_P LMC(t) + \gamma_P SST(t), \quad (9)$$

228 respectively. The results for the coefficients  $\beta_T$ ,  $\gamma_T$ ,  $\beta_P$  and  $\gamma_P$  are shown in Table 1. For all cases, the linear  
 229 regression captures most of the signal ( $R^2$  is close to 1). Even though the large-scale variability is similar for all  
 230 the variables (Fig. 7), the precipitation variability is found to be much closer to the LMC variability than to the  
 231 SST variability ( $\beta_P \gg \gamma_P$ ). The dependence of the air temperature on the LMC and SST is less clear, but overall  
 232 it can be seen that the air temperature is better correlated with the SST ( $\gamma_T > \beta_T$ ). Therefore, the mechanism  
 233 governing the precipitation variability, while being mostly a result of the ENSO condition, is likely mediated by the  
 234 LMC variability.

235 While the LMC variability is closely related to the SST anomalies, it might also be influenced by other atmo-  
 236 spheric phenomena such as the Madden-Julian Oscillation [MJO, *Madden and Julian*, 1971; *Zhang*, 2005]. The need  
 237 for an explanation of the LMC modes beyond the SST is most evident in  $C_2$  and  $C_3$ , in which the LMC is different  
 238 by the equivalent signal in the SST is similar. This need might also exist for the other clusters. To examine the  
 239 connection of the LMC clusters to the MJO, we choose here to represent the MJO state using the daily outgoing  
 240 long-wave radiation (OLR), bandpass filtered between 10-90 days. Taking the monthly averages of the daily data  
 241 allows us to calculate the OLR composites for each cluster (Fig. 8). We again calculate the non-parametric 95%  
 242 significance level for all longitudes. While the typical amplitude of the MJO composites is an order of magnitude  
 243 smaller than that of the monthly climatology of the OLR field, OLR composites for clusters 2 to 5 include regions  
 244 in which the composite value is statistically significant, and more importantly, the structure of the signals resembles  
 245 different phases of the MJO [*Wheeler and Hendon*, 2004]: cluster 2 is similar to MJO phase 6, cluster 3 is similar  
 246 to MJO phases 2 and 3, and clusters 4 and 5 are similar to MJO phase 5. While the connection of the El-Niño  
 247 related cluster ( $C_4$  and  $C_5$ ) to the MJO is overall similar, the two La-Niña related clusters ( $C_2$  and  $C_3$ ) are related  
 248 to opposite phases of the MJO. The dependence of the LMC on the MJO is revealed by calculating the multilinear  
 249 regression

$$LMC(t) = \alpha_L + \beta_L MJO(t) + \gamma_L SST(t) \quad (10)$$

250 (Table 1, last 3 columns). Aside from cluster 1, all the apparently ENSO related clusters are better explained when  
 251 the MJO is included in the regression, with around 25% contribution from the MJO states. The fact that the LMC  
 252 clusters are significantly correlated with the MJO suggests that the LMC is affected by the MJO activity in addition

	Air Temperature			Precipitation			LMC		
	LMC ( $\beta_T$ )	SST ( $\gamma_T$ )	$R^2$	LMC ( $\beta_P$ )	SST ( $\gamma_P$ )	$R^2$	MJO ( $\beta_L$ )	SST ( $\gamma_L$ )	$R^2$
$C_1$	0.21	0.39	0.33	0.81	0.09	0.78	0.08	0.80	0.64
$C_2$	0.16	0.77	0.82	0.89	0.06	0.88	0.24	0.82	0.74
$C_3$	0.17	0.73	0.75	0.87	0.06	0.85	0.26	0.76	0.65
$C_4$	0.06	0.83	0.88	0.72	0.26	0.89	0.21	0.84	0.75
$C_5$	0.14	0.66	0.61	0.81	0.15	0.87	0.21	0.83	0.74

Table 1: Dependence of air temperature and precipitation on the LMC and SST (Eqs. 8,9), and the dependence of the LMC on the MJO and the SST (Eq. 10), for the 5 clusters. Shown are the multi-linear regression coefficients. Also shown is the  $R^2$  for each case.

to the SST. This result is consistent with the findings of several other studies [e.g., *Seo et al.*, 2016; *Schwendike et al.*, 2021].

## 4 Discussion and conclusion

The Hadley circulation is a key element of the climate system, which is responsible for the energy and moisture transport from the equatorial region to the subtropics. It is commonly defined as the zonally-averaged meridional circulation in the tropical region and is usually calculated as an annual mean or as an average over specific months or seasons. In recent years, several studies looked at the longitudinal dependence of the meridional circulation via decomposition of the three-dimensional atmospheric flow into local meridional and zonal flows using a Helmholtz decomposition into divergent and rotational flows, enabling the examination of the meridional circulation at each longitude separately. This allows to quantitatively distinguish, for example, between the Hadley circulation in the west Pacific and the Walker circulation in the equatorial Pacific [*Schwendike et al.*, 2014, 2015]. These studies gave useful analysis of the regionality and variability of the meridional circulation, yet their spatial analysis did not consider the east-west movement of the large-scale tropical circulation, and the interannual temporal variability examined was limited to assumed connection to variability modes such as ENSO.

In this study we investigated the interannual variability of the longitudinal-dependent meridional circulation (LMC), using hierarchical clustering, and a Lagrangian perspective that allows the identification of the actual large-scale circulation in the tropics. We find that the interannual variability can be represented by 5 clusters, all showing that the most prominent interannual variability of the LMC is due to a shift in the east-west direction of the circulation. This variability is found to be strongly related to other climatic variables such as the sea surface temperature, precipitation and air temperature. Using a method of tracking air parcels, we reveal the full changes in the interannual tropical circulation. We find that the east-west movement of the circulation is indeed the main variability on interannual time scales, and that the LMC is dominant in setting the 3D circulation and its variability. We also relate the LMC interannual variability to the Madden-Julian Oscillation (MJO) and find that the 2 La-Niña related modes are significantly correlated with 2 different MJO phases.

*Acknowledgements:* This research has been supported by the Israeli Science Foundation (Grant 996/20), and the Weizmann Institute Helen Kimmel Center for Planetary Science. ET is supported by the NSF Climate and Large-Scale Dynamics program, grant AGS-1826635, and thanks the Weizmann Institute for its hospitality during parts of this work. Data is available via the Harvard Dataverse: <https://doi.org/10.7910/DVN/KTBSCZ>

## References

- Cheng, X., and J. M. Wallace, Cluster Analysis of the Northern Hemisphere Wintertime 500-hPa Height Field: Spatial Patterns., *J. Atmos. Sci.*, 50(16), 2674–2696, doi:10.1175/1520-0469(1993)050<2674:CAOTNH>2.0.CO;2, 1993.
- Dee, D., et al., The ERA-Interim reanalysis: configuration and performance of the data assimilation system, *Q. J. R. Meteorol. Soc.*, 137(656), 553–597, doi:10.1002/qj.828, 2013.
- Feldstein, S. B., and S. Lee, Intraseasonal and interdecadal jet shifts in the northern hemisphere: The role of warm pool tropical convection and sea ice, *J. Climate*, 27(17), 6497–6518, doi:10.1175/JCLI-D-14-00057.1, 2014.

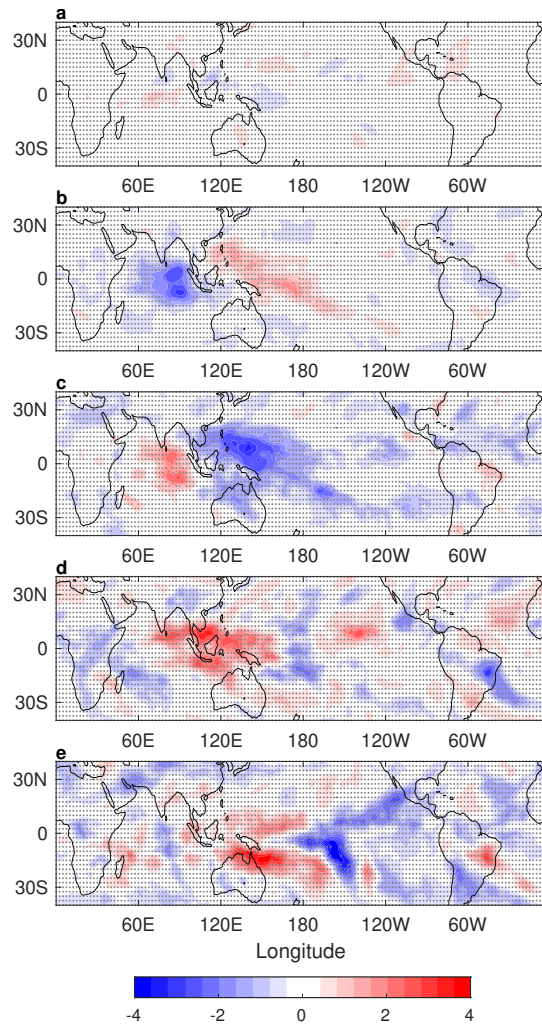


Figure 8: As in Fig. 4 but for composites of 10-90 days bandpass OLR ( $\text{W m}^{-2}$ ). Regions below the 95% confidence level are marked with gray dots.

- 290 Hartmann, D. L., *Global Physical Climatology*, Academic Press, 1994.
- 291 Hartmann, D. L., Chapter 6 - atmospheric general circulation and climate, in *Global Physical Climatology (Second*  
 292 *Edition)*, second edition ed., pp. 159 – 193, Elsevier, Boston, 2016.
- 293 Horton, D. E., N. C. Johnson, D. Singh, D. L. Swain, B. Rajaratnam, and N. S. Diffenbaugh, Contribution of  
 294 changes in atmospheric circulation patterns to extreme temperature trends, *Nature*, *522*(7557), 465–469, doi:  
 295 10.1038/nature14550, 2015.
- 296 Hu, S., J. Cheng, and J. Chou, Novel three-pattern decomposition of global atmospheric circulation: generalization  
 297 of traditional two-dimensional decomposition, *Clim. Dyn.*, *49*(9-10), 3573–3586, doi:10.1007/s00382-017-3530-3,  
 298 2017.
- 299 Kanamitsu, M., W. Ebisuzaki, J. Woollen, S.-K. Yang, J. J. Hnilo, M. Fiorino, and G. L. Potter, NCEP-DOE  
 300 AMIP-II Reanalysis (R-2)., *Bull. Am. Meteor. Soc.*, *83*(11), 1631–1643, doi:10.1175/BAMS-83-11-1631, 2002.
- 301 Karneuskas, K. B., and C. C. Ummenhofer, On the dynamics of the Hadley circulation and subtropical drying,  
 302 *Clim. Dyn.*, *42*(9), 2259–2269, doi:10.1007/s00382-014-2129-1, 2014.
- 303 Keyser, D., B. D. Schmidt, and D. G. Duffy, A technique for representing three-dimensional verti-  
 304 cal circulations in baroclinic disturbances, *Mon. Weath. Rev.*, *117*(11), 2463–2494, doi:10.1175/1520-  
 305 0493(1989)117<2463:ATFRTD>2.0.CO;2, 1989.

- 306 Madden, R., and P. Julian, Detection of a 40-50 day oscillation in the zonal wind in the tropical pacific, *J. Atmos.*  
307 *Sci.*, 28(5), 702–708, doi:10.1175/1520-0469(1971)028<0702:DOADOI>2.0.CO;2, 1971.
- 308 Madonna, E., C. Li, C. Grams, and T. Woollings, The link between eddy-driven jet variability and weather regimes  
309 in the north Atlantic-European sector, *Q. J. R. Meteorol. Soc.*, 143(708), 2960–2972, doi:10.1002/qj.3155, 2017.
- 310 Nguyen, H., A. Evans, C. Lucas, I. Smith, and B. Timbal, The Hadley Circulation in Reanalyses: Climatology,  
311 Variability, and Change, *J. Climate*, 26(10), 3357–3376, doi:10.1175/JCLI-D-12-00224.1, 2013.
- 312 Nguyen, H., H. H. Hendon, E. P. Lim, G. Boschhat, E. Maloney, and B. Timbal, Variability of the extent of the Hadley  
313 circulation in the southern hemisphere: a regional perspective, *Clim. Dyn.*, 50(1), 129–142, doi:10.1007/s00382-  
314 017-3592-2, 2018.
- 315 Raiter, D., E. Galanti, and Y. Kaspi, The Tropical Atmospheric Conveyor Belt: A Coupled Eulerian-Lagrangian  
316 Analysis of the Large-Scale Tropical Circulation, *Geophys. Res. Lett.*, 47(10), e86437, doi:10.1029/2019GL086437,  
317 2020.
- 318 Schwendike, J., P. Govekar, M. J. Reeder, R. Wardle, G. J. Berry, and C. Jakob, Local partitioning of the overturning  
319 circulation in the tropics and the connection to the Hadley and Walker circulations, 119(3), 1322–1339, doi:  
320 10.1002/2013JD020742, 2014.
- 321 Schwendike, J., G. J. Berry, M. J. Reeder, C. Jakob, P. Govekar, and R. Wardle, Trends in the local Hadley and  
322 local Walker circulations, 120(15), 7599–7618, doi:10.1002/2014JD022652, 2015.
- 323 Schwendike, J., G. J. Berry, K. Fodor, and M. J. Reeder, On the Relationship Between the Madden-Julian Oscillation  
324 and the Hadley and Walker Circulations, 126(4), e2019JD032,117, doi:https://doi.org/10.1029/2019JD032117,  
325 e2019JD032117 2019JD032117, 2021.
- 326 Seo, K., H. Lee, and D. Frierson, Unraveling the teleconnection mechanisms that induce wintertime temperature  
327 anomalies over the northern hemisphere continents in response to the MJO, *J. Atmos. Sci.*, 73(9), 3557–3571,  
328 doi:10.1175/JAS-D-16-0036.1, 2016.
- 329 Tanaka, H. L., N. Ishizaki, and A. Kitoh, Trend and interannual variability of Walker, monsoon and Hadley circula-  
330 tions defined by velocity potential in the upper troposphere, *Tellus A: Dynamic Meteorology and Oceanography*,  
331 56(3), 250–269, doi:10.3402/tellusa.v56i3.14410, 2004.
- 332 Totz, S., E. Tziperman, D. Coumou, K. Pfeiffer, and J. Cohen, Winter precipitation forecast in the eu-  
333 ropean and mediterranean regions using cluster analysis, *Geophys. Res. Lett.*, 44(24), 12,418–12,426, doi:  
334 10.1002/2017GL075674, 2017.
- 335 Trenberth, K., and D. Stepaniak, Seamless poleward atmospheric energy transports and implications for the Hadley  
336 circulation, *J. Climate*, 16(22), 3706–3722, doi:10.1175/1520-0442(2003)016<3706:SPAETA>2.0.CO;2, 2003.
- 337 Trenberth, K. E., D. P. Stepaniak, and J. M. Caron, The global monsoon as seen through the divergent atmospheric  
338 circulation, *J. Climate*, 13(22), 3969–3993, doi:10.1175/1520-0442(2000)013<3969:TGMASST>2.0.CO;2, 2000.
- 339 Wheeler, M., and H. Hendon, An all-season real-time multivariate MJO index: Development of  
340 an index for monitoring and prediction, *Mon. Weath. Rev.*, 132(8), 1917–1932, doi:10.1175/1520-  
341 0493(2004)132<1917:AARMMI>2.0.CO;2, 2004.
- 342 Wilks, D., *Statistical methods in the atmospheric sciences*, pp. 100 pp., Academic Press, Waltham, USA, 2011.
- 343 Zhang, C., Madden-Julian Oscillation, *Rev. Geophys.*, 43(2), doi:10.1029/2004RG000158, 2005.
- 344 Zhang, G., and Z. Wang, Interannual variability of the Atlantic Hadley circulation in boreal summer and its impacts  
345 on tropical cyclone activity, *J. Climate*, 26(21), 8529–8544, doi:10.1175/JCLI-D-12-00802.1, 2013.